

Article

Parametric Study on Seismic Rehabilitation of Masonry Buildings Using FRP Based upon 3D Non-Linear Dynamic Analysis

Eissa Fathalla  and Hamed Salem *

Structural Engineering Department, Faculty of Engineering, Cairo University, Giza 12613, Egypt; eissa.tokyo.concrete@gmail.com

* Correspondence: hamedhadhoud@yahoo.com; Tel.: +20-1006044741

Received: 22 July 2018; Accepted: 30 August 2018; Published: 4 September 2018



Abstract: Unreinforced load-bearing masonry (URM) buildings represent a significant portion of the non-engineered old buildings in many developing countries aiming to reduce the construction cost. The walls of those buildings are developed to resist gravity loads. Lateral loads induced by earthquakes or wind may cause severe their damage. In the current study, a numerical investigation is carried out for a seismic assessment of a typical four-story, load-bearing building in Giza, Egypt. The full 3D nonlinear dynamic analysis is carried out using the Applied Element Method (AEM), which proved to be efficient in such case where partial or total collapse is expected. The study includes two earthquake zones in Egypt called zone (3) and zone (5B), which are the actual studied building seismic zone and the highest seismic activity zone in Egypt, respectively. Carbon fiber reinforced polymers (CFRP) laminates with different thicknesses and different configurations are used in strengthening unreinforced masonry walls to study the efficiency of the proposed rehabilitation technique on a realistic structure.

Keywords: AEM; load-bearing masonry walls; seismic rehabilitation

1. Introduction

Load-bearing masonry buildings represent a significant portion of the old buildings in Egypt. Those buildings are mostly non-engineered and constructed without engineering supervision. Their walls are mainly used to resist gravity loads. Lateral loads induced by earthquakes (EQ) or the wind are not taken into account; therefore they may cause severe structural damages. Therefore, seismic rehabilitation of such buildings is believed to be crucial for upgrading their lateral capacity. They also may need to be upgraded to meet more extreme design seismic requirements.

Currently, many researchers focus on the use of innovative strengthening techniques involving fiber reinforced polymers (FRP) materials [1]. FRP can be used for strengthening structural members in the form of laminates or sheets. It appears that the use of FRP composites to strengthen unreinforced masonry walls might be a powerful technique to enhance both in-plane and out of plane behavior of walls where it was investigated in previous research studies both experimentally and numerically [2–12].

In the current study, a numerical investigation is carried out for seismic rehabilitation of a four-story, load-bearing building located in Giza, Egypt by using carbon a fiber reinforced polymer (CFRP). The magnitude of earthquakes used in the current study is according to the Egyptian design code for loads [13]. The study includes two earthquake zones in Egypt known as zone (3) and zone (5B) with design magnitudes of 15% and 30% of the gravitational acceleration, respectively. The full 3D nonlinear dynamic analysis is carried out using the Applied Element Method (AEM) [14]. The AEM is based on a discrete crack approach and is capable of predicting the nonlinear structural behavior as

well as local damage and total collapse. Therefore, it is believed to be efficient for the current study where partial or total collapse is expected. CFRP laminates with different thicknesses and different configurations are used in strengthening the URM walls to study the efficiency of the proposed strengthening technique.

2. The Applied Element Method

The AEM simulates the structure by virtually dividing it into small elements that are connected by normal and shear springs positioned at specific contact points around the surface of the elements [14]. Each assembly of springs represent the deformations and stresses of a particular volume. The AEM has been considered a reliable method to track the collapse of structures passing through all the phases of the application of loads, elastic stage, cracking initiation, reinforcement yield, rupture, elements separation, and collision with ground and adjacent structures. Maekawa's compression model [15] is used for concrete modeling under compression, which is shown in Figure 1a. For concrete shear springs, the linear relation of shear stress and shear strain is assumed until the cracking of concrete occurs. Then the shear stresses drop, as shown in Figure 1b. The level of the drop depends on aggregate interlocking and friction at the crack surface. For reinforcement springs, Figure 2 shows the model, which is previously presented for cyclic loading of reinforcing steel bars [16] and is used in AEM. The authors utilize the constitutive models of concrete to simulate the masonry structure in which they both have the same general trend [17]. Moreover, we validate our method by previous experimental program, where the validation results are shown in the following section.

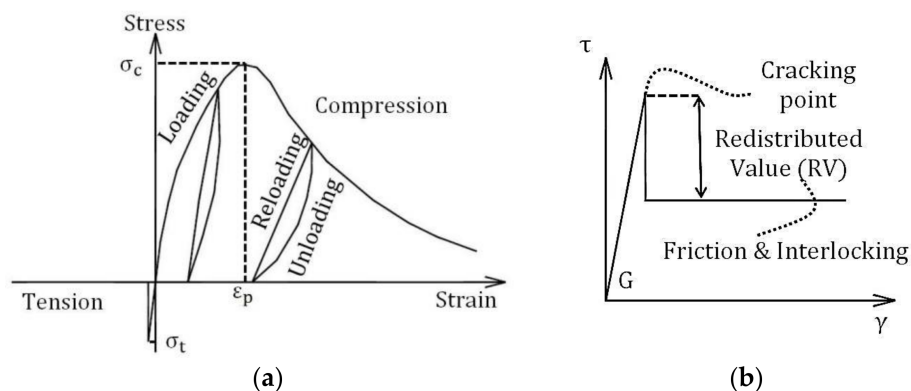


Figure 1. (a) Axial stresses in concrete springs due to relative displacement. (b) Shear stresses in concrete springs due to relative displacement.

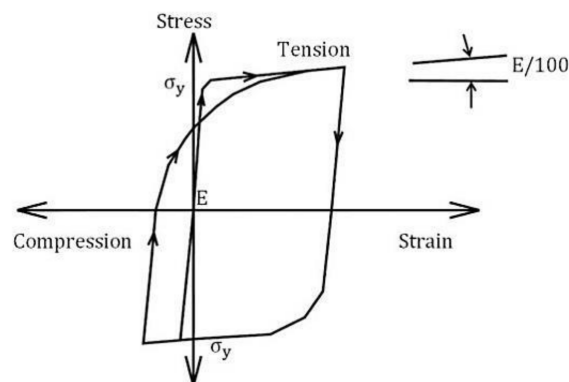


Figure 2. Stresses in steel springs due to relative displacement.

Although the Finite Element Method (FEM) is a well-established and robust structural analysis method, it may not be the optimum solution for the scope of the present study. Many drawbacks are

associated with the FEM progressive collapse analysis. The elements' separation, falling, and collision with each other are complicated to simulate. Previous research studies [18–20] showed that the computations associated with the simulation of collapses of real structures based on conventional FEM are very costly; therefore they followed another approach based on multibody models. Even though the progressive collapse analysis is possible in the explicit-integration FEM [21,22], it still has drawbacks that the element separation is introduced through erosion of highly stressed elements and the element's size should be as small as possible to enable such erosion acceptably, which causes the computations to be very costly and impractical when analyzing real structures. Additionally, cracks are introduced due to these elements' erosion, where the crack width equals to the removed elements' size. Thus, no shear transfer is possible across the crack surface and there is no opportunity for the crack closure, which does not allow correct modelling of members' seismic behavior. Consequently, in the current study, the numerical analysis was carried out using the AEM, where it is widely validated and has shown considerable agreement with real cases. It also covers many cases such as static, dynamic, and collapse cases [22–34]. The software used in the analysis is Extreme Loading for Structures (ELS[®], Charlotte, NC, USA) [35], which is based on the AEM.

3. Validation of the Analysis Method

The experimental results of Santa Maria et al. [8] are used for validating the AEM results. Santa Maria et al. [8] carried out an experimental program to study the behavior of masonry walls externally reinforced with CFRP and subjected to in-plane cyclic loading. This experiment was carried out on six full-scale masonry walls. Two of the walls were not retrofitted (control) and the rest were retrofitted with CFRP strips that have different configurations and reinforcement areas, which are shown in Table 1 and Figure 3. The specimens were subjected to an in-plane cyclic load under a constant uniformly distributed vertical load of 98 kN. The loading setup of the experiment is shown in Figure 4.

Table 1. CFRP reinforcement of the tested walls [8].

Specimen Name	Reinforcement Configuration	Strip Width (mm)	Total Area of Reinforcement (m ²)	Ratio of FRP Reinforcement (%)
MLC-00-CA-SF-01	-	-	-	-
MLC-00-CA-SF-02	-	-	-	-
MLC-00-CA-FX-01	Diagonal	300	3.37	0.2
MLC-00-CA-FX-03	Diagonal	200	2.25	0.13
MLC-00-CA-FH-02	Horizontal	150	1.78	0.42
MLC-00-CA-FH-04	Horizontal	100	1.19	0.28

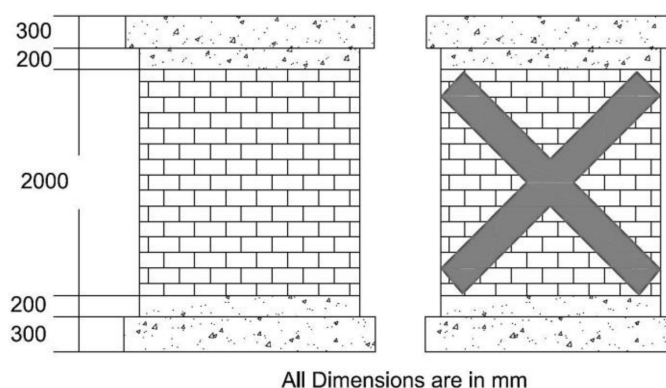


Figure 3. Configuration of exterior reinforcement for the experimental program [8].

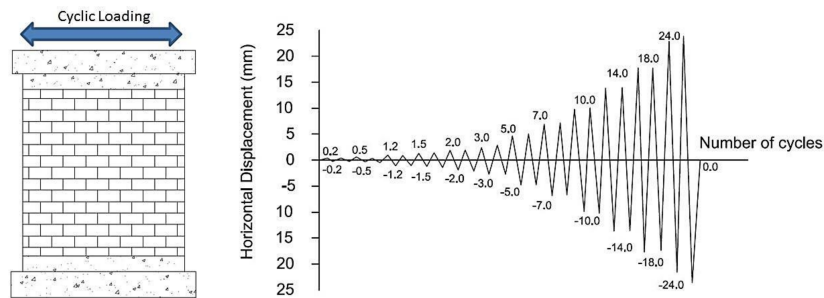


Figure 4. Horizontal displacement program for the cyclic shear tests [8].

The tested specimens were modeled using ELS software (version 3.1, Applied Science International, Morrisville, NC, USA). Two models are adopted for each tested wall, which are described below.

1. Walls are modeled with real brick configurations and connected with mortar joints (Masonry mesh), which is shown in Figure 5.
2. Walls are modeled with simplified quadrilateral mesh including average properties of brick and mortar, which is shown in Figure 6 where the masonry wall is divided in the wall plane to 40×40 discretized elements.

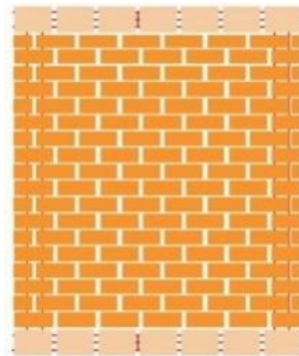


Figure 5. Walls modeled as masonry mesh.

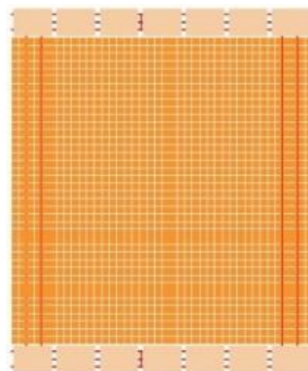


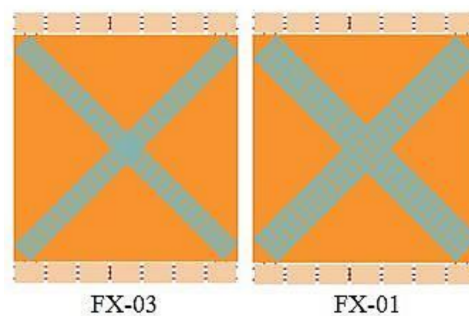
Figure 6. Walls modeled as simplified mesh 40×40 .

The Material properties of the masonry are shown in Table 2. Since the CFRP laminates are not expected to carry compressive forces, the compressive strength is chosen to be a small value (0.35 N/mm^2) in order to permit simulation's computations. Interface elements are utilized in the simulation program for modeling the epoxy material in which the de-bonding of the CFRP laminates can be simulated if it occurs.

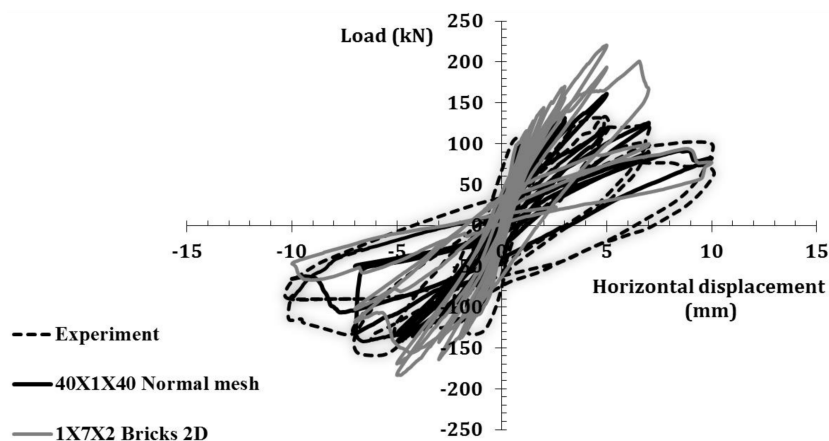
Table 2. Material properties of the experimental program.

Material Type		Bricks	Mortar	CFRP (0.13 mm)	Epoxy
Young's Modulus	N/mm ²	6618	10,000	230,000	3000
Compressive Strength	N/mm ²	11	25	-	80
Tensile Strength	N/mm ²	0.85	5	3500	50
Specific Weight	kN/m ³	18	22	19	12

For the masonry mesh, two materials were used including one for bricks and the other for mortar. The stiffness of the material used in the case of modeling walls as simplified mesh was an average of mortar and bricks. Since bricks were weaker than mortar, cracking was governed by bricks. Figure 7 shows the numerical model for the retrofitting scheme of the walls using CFRP, where the CFRP are attached to the walls using an epoxy adhesive material.

**Figure 7.** Configuration of exterior reinforcement for the numerical model.

A comparison of hysteresis loops of tested walls for both the experimental model and the numerical model for the masonry panel (SF-01 or SF-02), (FX-01), and (FX-03) are shown in Figures 8–10, respectively. The obtained results show that the AEM with utilizing the concrete constitutive laws is an acceptable and reasonable accurate method for the analysis of the masonry walls. It is evident that the experimental and the numerical model are in close agreement for both the masonry mesh and the simplified mesh (40 × 40). Therefore, it is decided to use the simplified mesh for the modeling of masonry walls to reduce the problem size for the full-scale model analysis of the multi-story building.

**Figure 8.** Comparison of experimental and analytical results for the URM wall (SF-01 or SF-02).

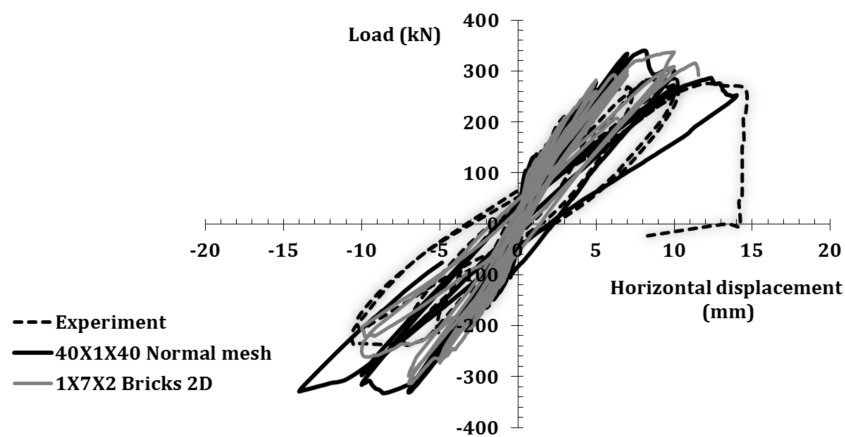


Figure 9. Comparison of experimental and analytical results for the FX-01 wall panel.

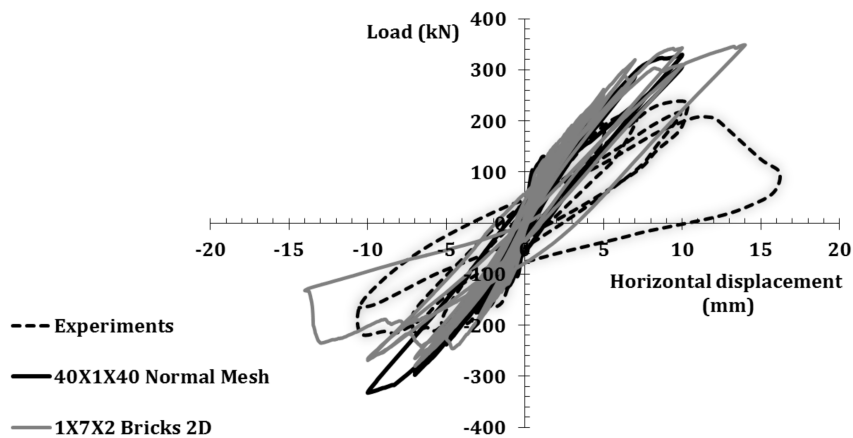


Figure 10. Comparison of experimental and analytical results for the FX-03 wall panel.

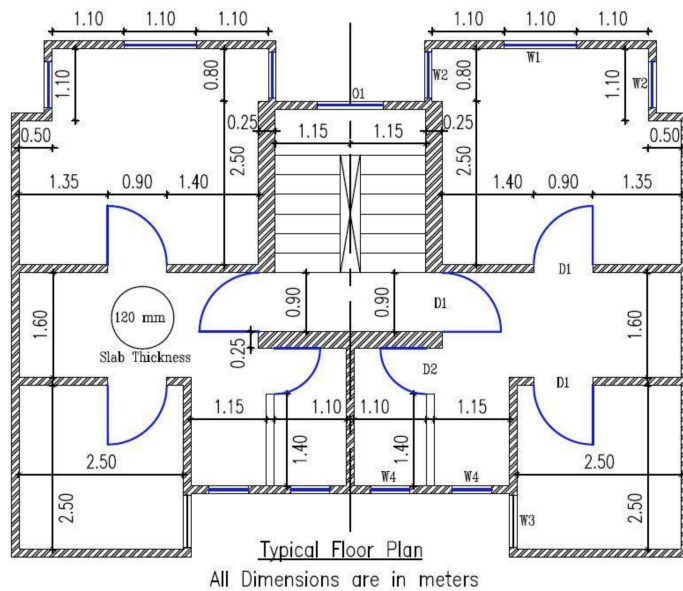
4. Case Study

4.1. Description of the Studied Structure

The investigated case study is an existing four-story residential building located in the Faisal district in Giza, Egypt and is constructed with load-bearing masonry walls. Figure 11 shows a picture of the building while Figure 12 shows the plan of the typical floor showing dimensions of walls (W), doors (D), and openings (O). All floors are 3 m high. Since no data is available for the reinforced concrete (RC) slab reinforcement, bottom reinforcement is reasonably assumed with a diameter of 8 mm and 200 mm spacing in both directions along with an additional top reinforcement with a diameter of 8 mm and 200 mm spacing, as shown in Figure 13. It should be noted that the staircase is omitted in the model for simplicity. The RC slabs are supported on RC beams at the walls locations, where these beams are directly supported on the masonry bearing walls, which is similar to a prior construction practice in Egypt. A detailed three-dimensional model is built using ELS by taking into consideration all structural components. Figure 14 shows different views of the numerical model.



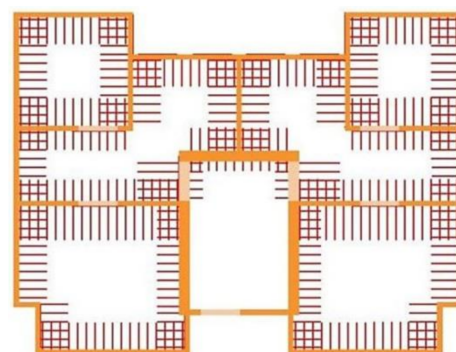
Figure 11. Case study building.



Note: All Masonry walls are 120 mm except mentioned

Type	Dimensions (mm)		
	Length	Width in plan	Height from floor
D1	2200	900	---
D2	2200	700	---
W1	1200	1100	1100
W2	1200	700	1100
W3	1200	800	900
W4	1000	600	1100
O1	1000	1000	Above floor level

Figure 12. Typical floor plan of the studied case.



Bottom Reinforcement
D8@ 200 mm

Additional
Top Reinforcement
As shown in figure
D8@ 200 mm

D: Rebar's diameter

Figure 13. Reinforcement details of the reinforced concrete slabs.

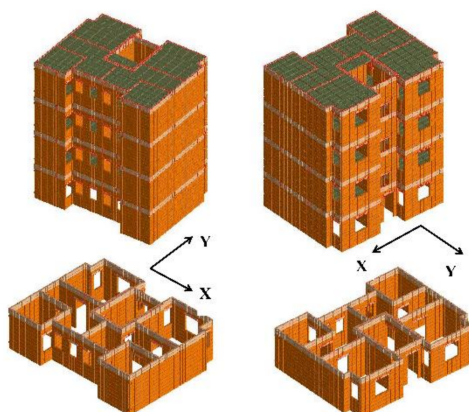


Figure 14. Different views of the numerical model.

4.2. Material Properties

Properties of concrete, reinforcement, bricks, CFRP (width = 0.5 m and thickness = 0.5 mm), and epoxy are listed in Table 3.

Table 3. Material properties of the studied case.

Material Type		Concrete	Bricks	CFRP	Epoxy	Steel Reinforcement
Young's Modulus	N/mm ²	22,000	6618	230,000	3000	200,000
Compressive Strength	N/mm ²	25	10	0.35	80	-
Tensile Strength	N/mm ²	2.5	1	3500	50	360
Specific Weight	kN/m ³	25	19	18	12	78
Ultimate Strength	N/mm ²	-	-	-	-	520

4.3. Loads

The self-weight of the structure, the floor weight, the live loads, and the earthquake load are applied to the studied structure. The floor and live loads on the slabs are considered equal to 2.0 kN/m² and 2.5 kN/m², respectively. The ultimate load combination given by the ECP [13] is used (1.12 D.L + 0.25 L.L + S) where D.L is the dead load, L.L is the live load, and S is the seismic load. The coupled orthogonality effect is not considered in this paper in order to study the effect of strengthening of each direction separately. This load combination is applied to the building for 20 s, which is the duration of the applied earthquake.

4.4. Earthquake (EQ) Characteristics

In the current research, two earthquake magnitudes are considered.

1. First case. Design earthquake magnitude according to the actual location of the building in Giza (Zone 3), where the peak ground acceleration equals 0.15 g.
2. Second case. Design earthquake magnitude according to the most active seismic location in Egypt (zone 5B), where the peak ground acceleration equals 0.3 g.

Artificial acceleration time history records are created from the response spectrum using SIMQKE software (version 2.1, Massachusetts Institute of Technology, Cambridge, MA, USA) [36], as shown in Figure 15. The basis of SIMQKE software is creating random amplitudes and phase angles derived from a stationary power spectral density function of the motion. An envelope function of the form, shown in Figure 16, [36] is used to simulate the transient character of a real earthquake.

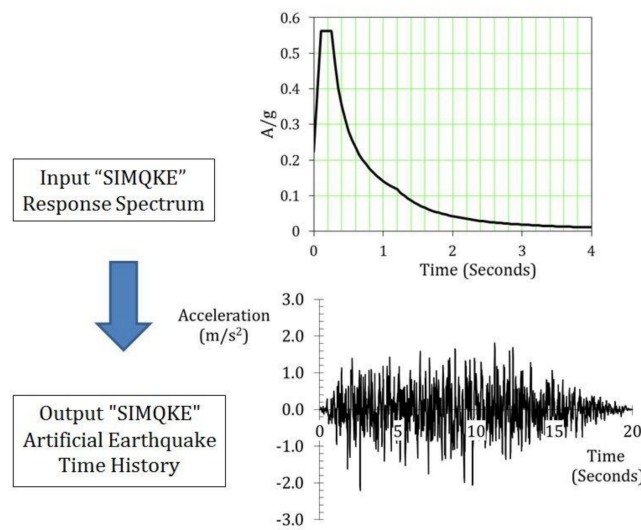


Figure 15. (SIMQKE) software conversion from response spectrum to earthquake time history acceleration [36].

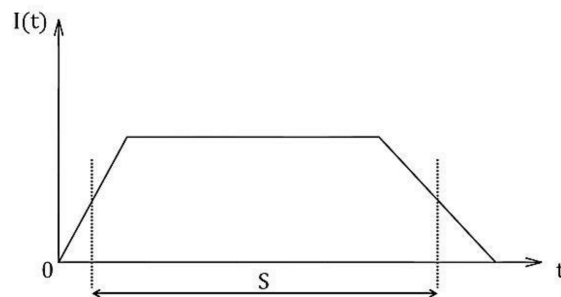


Figure 16. Intensity envelope function used to simulate the transient character of real earthquakes [36].

The simulated final motion $z(t)$ is shown Equation (1).

$$z(t) = I(t) \sum_{k=0}^n \sin(\omega_n t + \Phi_n) \quad (1)$$

$z(t)$: Simulated final motion; $I(t)$: Deterministic envelope function; n : The n th contributing sinusoid function; ω_n : Frequency content of the n th contributing sinusoid function; Φ_n : Phase angle of the n th contributing sinusoid function.

The final motion represented by Equation (1) represents a motion stationary in frequency content with maximum acceleration approximately equal to the target maximum acceleration. The software uses a frequency range bounded by $0.5 \omega_{low}$ and $2.0 \omega_{high}$, where ω_{low} and ω_{high} define the range for the required values of the response spectrum. The frequency step is $\omega_{n+1} = 0.005 \omega_n$, where it is purposed to be a fraction of the smallest value of half-bandwidth.

The elastic response spectra (RS) of the ECP design code and the utilized artificial earthquakes (produced by SIMQKE) of zone 3 and zone 5B [13] are shown in Figures 17 and 18, respectively. Figures 19 and 20 show the acceleration time history of earthquakes for both studied cases.

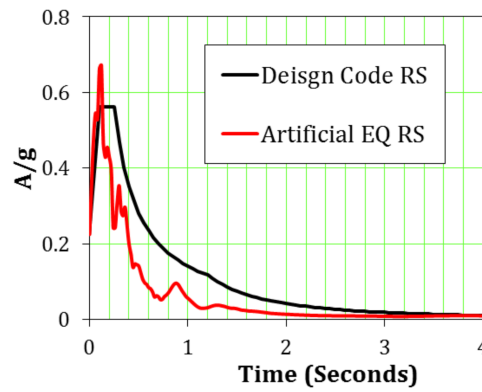


Figure 17. Design code and utilized artificial earthquake response spectrum of case (1).

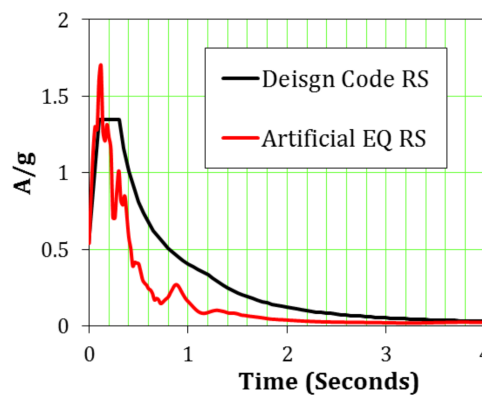


Figure 18. Design code and utilized artificial earthquake response spectrum of case (2).

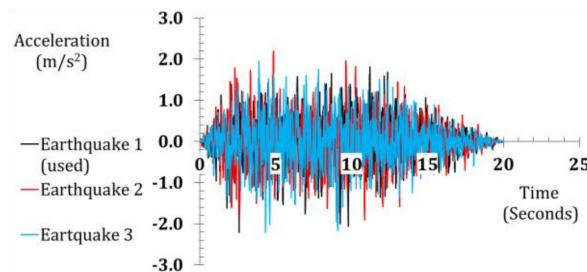


Figure 19. Acceleration time history of earthquakes in case (1).

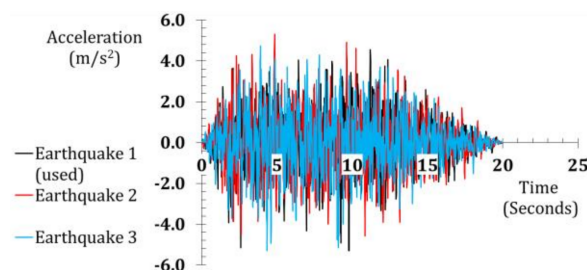


Figure 20. Acceleration time history of earthquakes in case (2).

4.5. Case Studies

Table 4 shows the studied cases where the building with non-retrofitted walls represents the reference case. In the retrofitted cases, the walls are retrofitted with CFRP laminates of width 0.5 m

and thickness 0.5 mm. Figures 21 and 22 show the retrofitting scheme for the walls in both cases including solid walls only and solid walls with openings, respectively. For solid walls, the CFRP is attached to the walls in the form of two intersecting diagonal strips. Since CFRP are not expected to resist compression forces, the two diagonal implementations are essential to resist the reversed cyclic loading during the earthquake application. As for the openings, the CFRP is attached in parallel to the sides of the openings.

Table 4. Studied cases.

Studied Cases (Legend)	Earthquake Direction	Earthquake Zone	Retrofitting Scheme
E.Q. X- ZONE 3	X	3	-
E.Q. Y- ZONE 3	Y	3	-
E.Q. X- ZONE 5B	X	5B	-
E.Q. Y- ZONE 5B	Y	5B	-
E.Q. X- ZONE 5B- SW	X	5B	Solid walls
E.Q. Y- ZONE 5B- SW	Y	5B	Solid walls
E.Q. X- ZONE 5B- SW & OP	X	5B	Solid walls & openings
E.Q. Y- ZONE 5B- SW & OP	Y	5B	Solid walls & openings

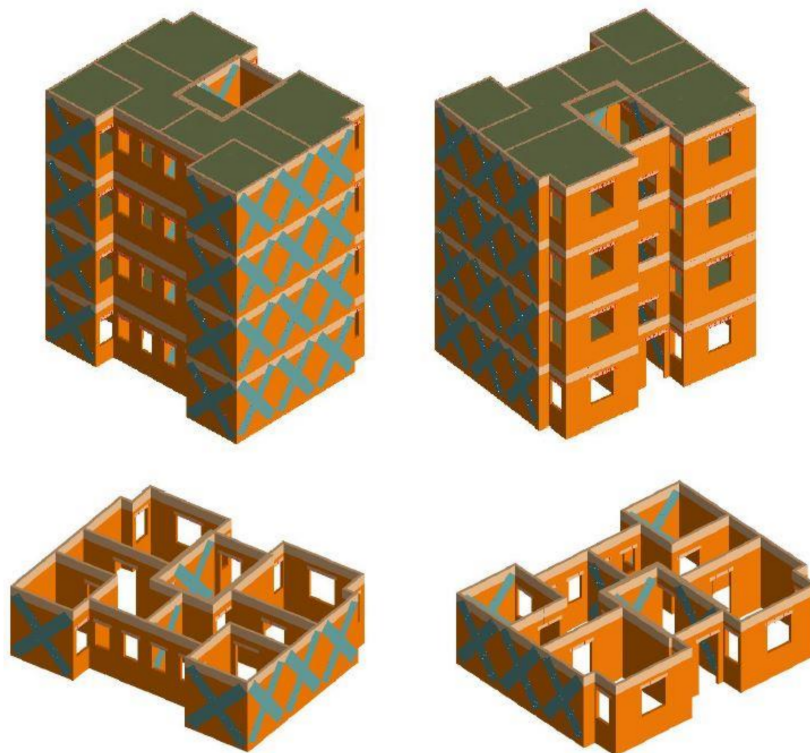


Figure 21. Retrofitting scheme (for solid walls only).

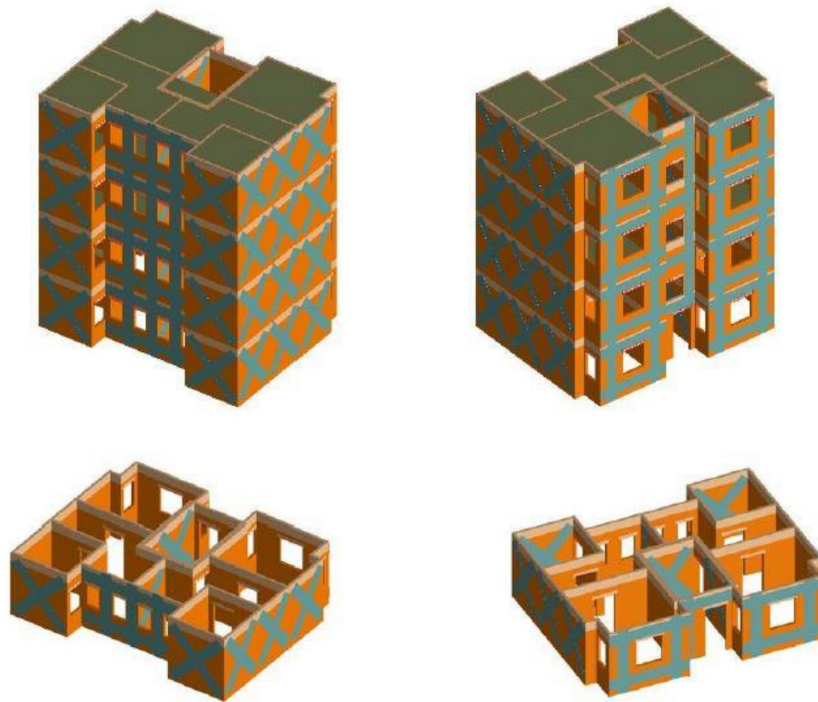


Figure 22. Retrofitting scheme for both solid walls and openings.

5. Numerical Results

The behavior of the studied building in resisting seismic loads and the efficiency of retrofitting using CFRP sheets are investigated with regard to the overall structural integrity, stability, and the damage level induced in the building due to the seismic action. In the following subsections, the deformed shapes of the studied building have a magnification factor of 20.

5.1. Reference (Non-Retrofitted) Case in Zone 3

As shown in Figures 23 and 24, the building is proven to maintain its global stability with minimal local damage during earthquake loading in the x-direction and the y-direction, respectively. The studied mid-rise masonry load-bearing building shows good behavior in resisting earthquakes in zone 3.

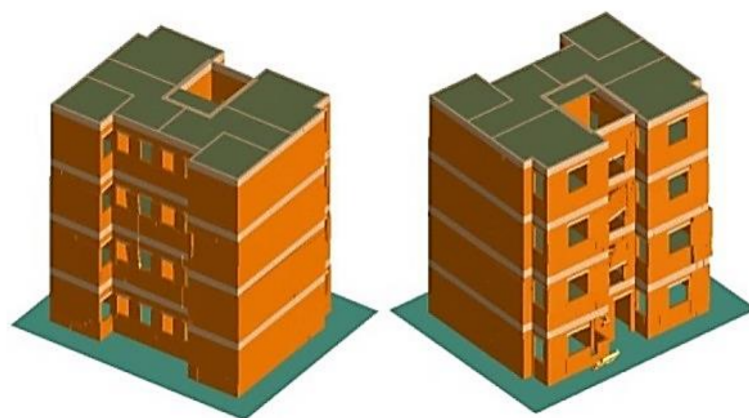


Figure 23. Deformed shape for the case (E.Q. X- ZONE 3).

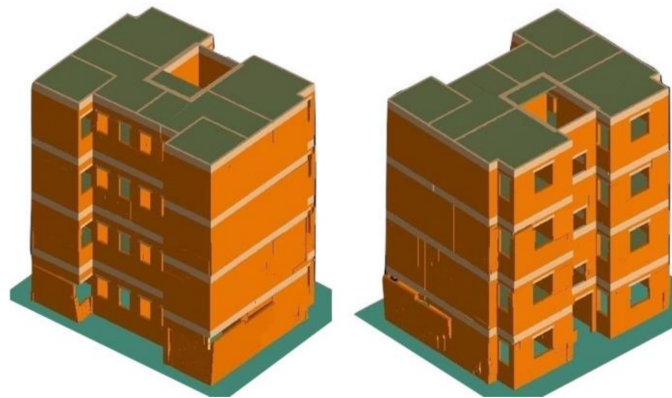


Figure 24. Deformed shape for the case (E.Q.Y- ZONE 3).

5.2. Reference (Non-Retrofitted) Case in Zone 5B

In this case, the building collapses entirely. A progressive collapse is observed for seismic loading in both directions, which is shown in Figures 25 and 26. The collapse starts by the failure of the bearing walls at the ground floor. In other words, the mid-rise masonry load-bearing building cannot resist earthquake loads for seismic zone 5B and retrofitting of the masonry walls would be necessary.

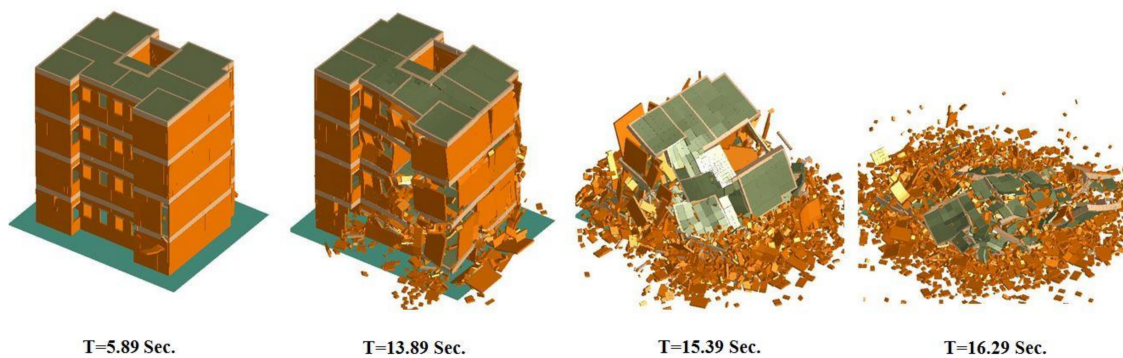


Figure 25. Progressive collapse of the building for the case study (E.Q. X- ZONE 5B).

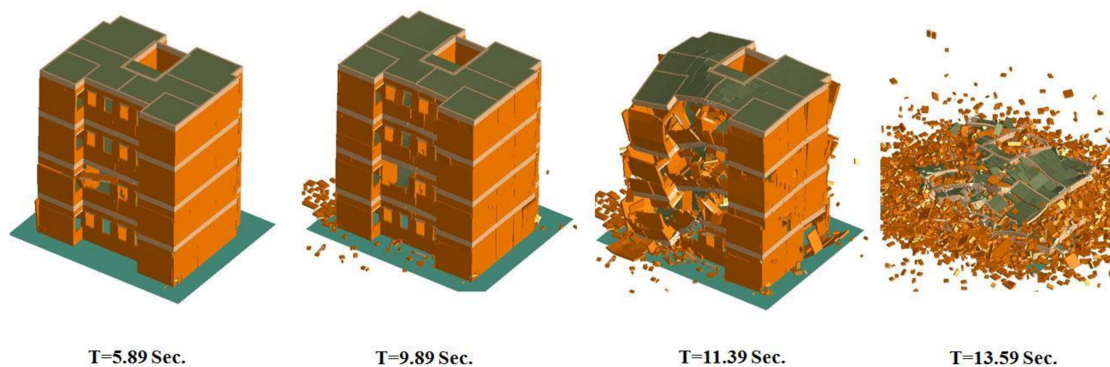


Figure 26. Progressive collapse of the building for the case study (E.Q.Y- ZONE 5B).

5.3. Case of Retrofitting Solid Walls in Zone 5B

Figures 27 and 28 show the final damage after the application of the earthquakes loading in the x-direction and the y-direction, respectively. The building is proven to maintain its global stability with the high local damage that occurs around the wall's opening. The externally bonded CFRP laminates

are proven to be an efficient technique for strengthening the masonry mid-rise walls bearing building subjected to seismic loads.

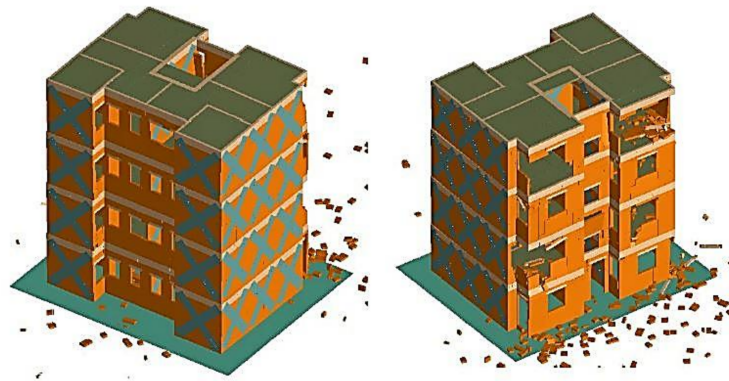


Figure 27. Damage obtained for the case study (E.Q. X- ZONE 5B- SW).

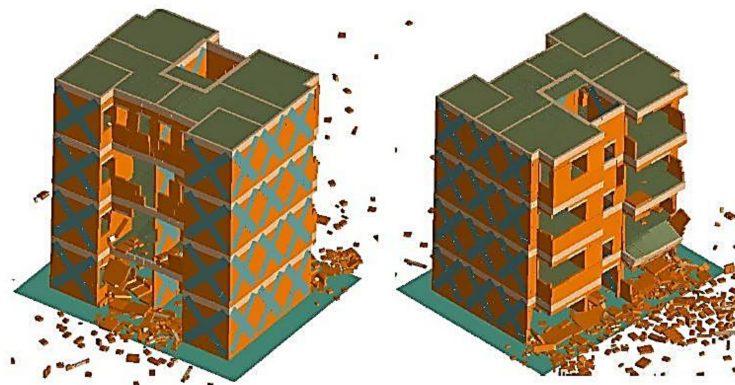


Figure 28. Damage obtained for the case study (E.Q. Y- ZONE 5B- SW).

Figure 29 shows the major principal strain contours at the ground floor walls for the case of the earthquake loading in the y-direction. The principal strain contours give a good indication of a cracking pattern with the lighter colors at the location of crack localization. Figure 30 shows the normal stresses versus time in the CFRP attached to one of the ground floor walls. As seen in Figure 30, the stresses in the CFRP do not reach its tensile strength (3500 N/mm^2) and the CFRP, therefore, do not rupture in the analysis. A sudden increase in the CFRP stresses is evident at time equals to 2.0 s. The sudden increase of the FRP stresses is explained by the crack occurrence in the walls at the location of the CFRP laminate, which could successfully bridge the crack and eventually maintain the wall stability.

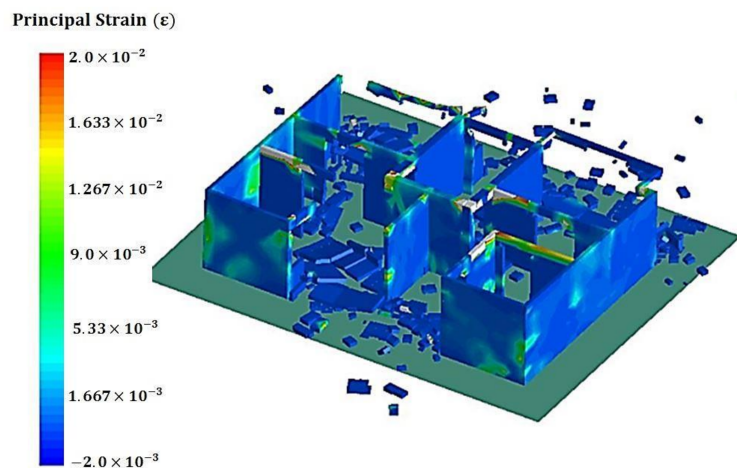


Figure 29. Principal strain contours of walls at the ground floor.

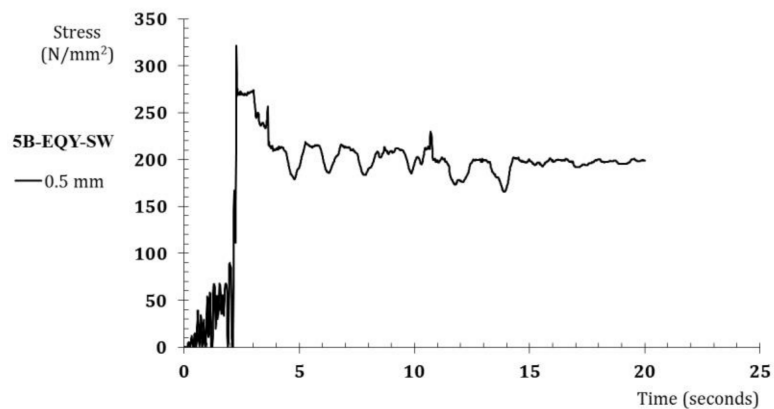


Figure 30. Normal stresses versus time for CFRP laminates at the ground floor.

5.4. Case of Retrofitting Solid Walls and Openings in Zone 5B

Numerical results verified that the building could successfully maintain its global stability with minor local damage, which is illustrated in Figures 31 and 32. The building's overall high stability proves the efficiency of the proposed strengthening technique of the current case study.

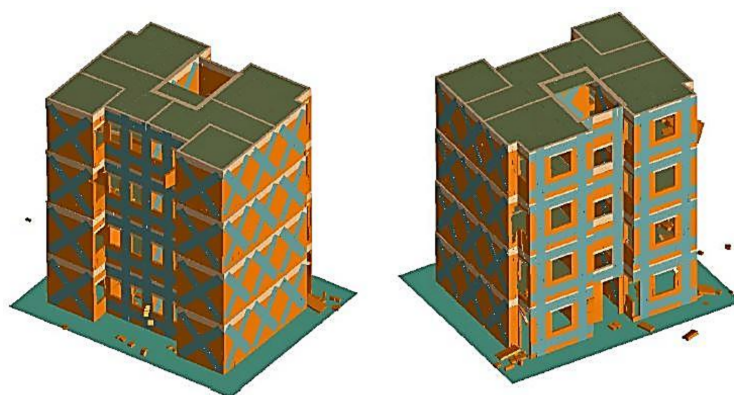


Figure 31. Deformed shape for the case study (E.Q. X- ZONE 5B- SW & OP).

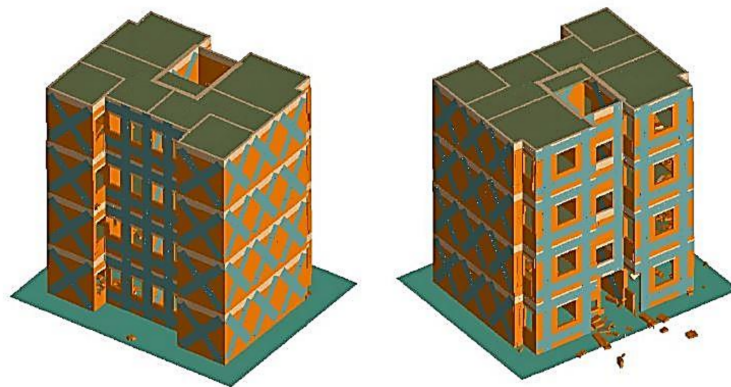


Figure 32. Damage obtained for the case study (E.Q. Y- ZONE 5B- SW & OP).

5.5. Optimization of the Amount of CFRP

Different thicknesses of CFRP (0.25, 1, and 1.5 mm) are used in the analysis of the retrofitted solid walls case to determine the minimum thickness of the CFRP laminates. Figures 33–36 show the sample of analysis results for the case (E.Q. X- ZONE 5B- SW). As seen in Figure 33, the lateral displacement at the top of the building decreases to almost half when CFRP thickness increases from 0.25 to 1.5 mm. The reason for such a reduction in displacement is that the CFRP reduces the induced cracks from the earthquake motion especially at the locations of the CFRP laminates where it is clearly seen in the principal strain contours in Figure 29, which was shown previously in Section 5.3. However, the base shear does not show a remarkable change, as shown in Figure 34. Figure 35 illustrates the hysteresis base shear-displacement curves for the building regarding different thicknesses of the CFRP where it can be recognized that the behavior is the same with higher deformability in the 0.25 mm thickness case. Figure 36 illustrates the stress versus time for the different CFRP thicknesses where the stresses in the CFRP of thickness 0.25 mm reach maximum value of 230.7 MPa, which is very much below the ultimate strength of the CFRP.

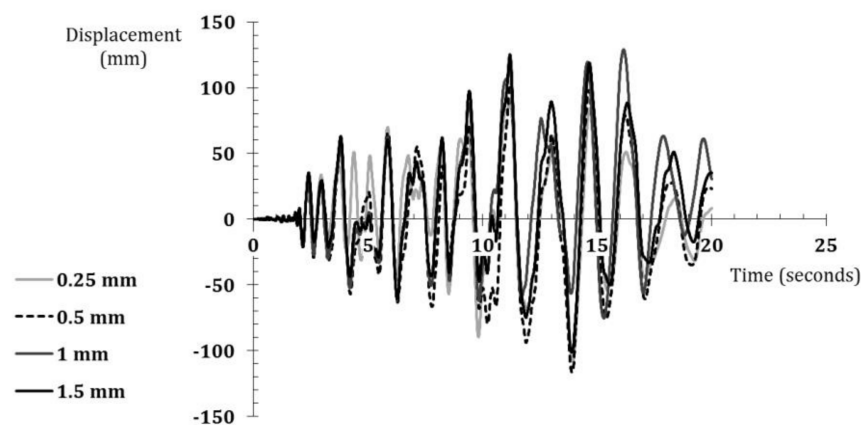


Figure 33. Effect of CFRP thickness. Top displacement vs. time for case (E.Q. X- ZONE 5B- SW).

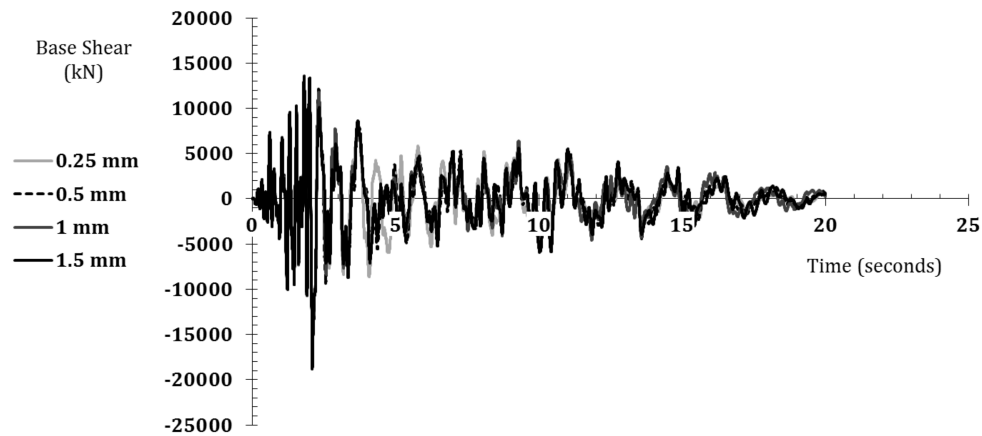


Figure 34. Effect of CFRP thickness. Base shear vs. time for case (E.Q. X- ZONE 5B- SW).

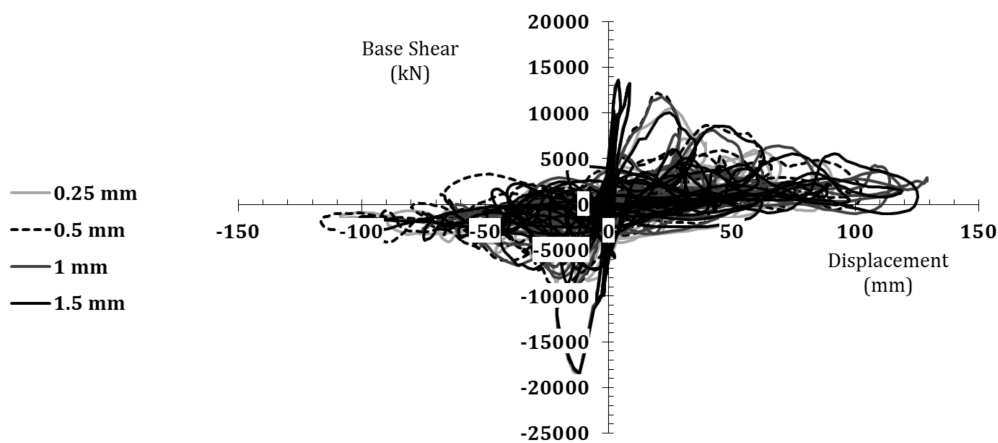


Figure 35. Effect of CFRP thickness. Base shear vs. top displacement for case (E.Q. X- ZONE 5B- SW).

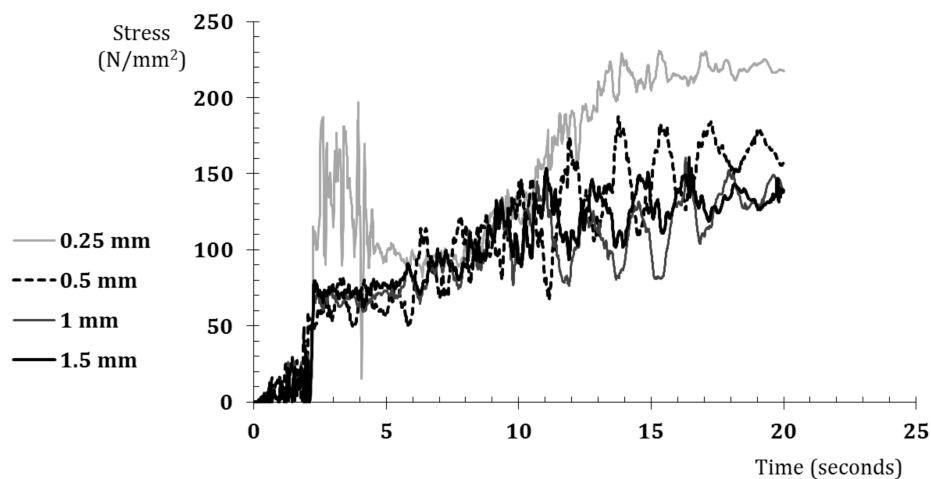


Figure 36. Effect of CFRP thickness. Normal stresses in CFRP versus time for case (E.Q. X- ZONE 5B- SW).

6. Conclusions

First, a validation is done for the experimental program of masonry walls under lateral loading by using the Applied Element Method simulation program. Afterward, a three-dimensional nonlinear dynamic analysis is carried out for numerically investigating the seismic rehabilitation of a typical masonry load-bearing residential building in Giza, Egypt by using carbon fiber reinforced polymer

(CFRP). The study included two earthquake zones in Egypt. Based on the results obtained from the studied cases, the following conclusions can be drawn.

- (1) On the basis of the validation results of the previous experimental program, the constitutive models of concrete can be used for simulating the masonry as simplification where the simulation results show good agreement with the experimental results.
- (2) The studied mid-rise masonry bearing walls building shows good behavior in resisting earthquakes for seismic zone 3 (peak ground acceleration of 0.15 g) while it shows a complete collapse in the seismic zone 5B (peak ground acceleration of 0.3 g).
- (3) The externally bonded CFRP laminates are proven to be efficient for seismically strengthening the masonry mid-rise bearing wall buildings. It shows a good capability of preventing structural collapse with minor local damage. For the current case study, strengthening with CFRP laminates of width 0.5 m and thickness 0.25 mm is proven to be sufficient for preventing the total collapse of the building.

Author Contributions: H.S. built the research scheme. E.F. collected the required information for the targeted existing structure. E.F. conducted the numerical simulations and analyzed the results. H.S. supervised the numerical process. E.F. and H.S. wrote the paper.

Funding: This research received no external funding.

Acknowledgments: The authors gratefully acknowledge Applied Science International, LLC, for granting the license of the simulation software (ELS[®]) to be used in the current research.

Conflicts of Interest: The authors declare no conflict of interest.

References

1. American Concrete Institution. *Abstract of: State of the Art Report on Fiber Reinforced Plastic (FRP) for Concrete Structures*; (ACI 440 R-95); American Concrete Institution: Farmington Hills, MI, USA, 1995; Volume 92, p. 5.
2. Stratford, T.; Pascale, G.; Manfroni, O.; Bonfiglioli, B. Shear Strengthening Masonry Panels with Sheet Glass-Fiber Reinforced Polymer. *J. Compos. Constr.* **2004**, *8*, 434–443. [[CrossRef](#)]
3. Petersen, R.B. In-Plane Shear Behavior of Unreinforced Masonry Panels Strengthened with Fiber Reinforced Polymer Strips. Ph.D. Thesis, The University of Newcastle, Callaghan, Australia, 2009.
4. Chuang, S.; Zhuge, Y.; Wong, T.; Peters, L. Seismic retrofitting of unreinforced masonry walls by FRP strips. In Proceedings of the Pacific Conference on Earthquake Engineering, University of Canterbury, Christchurch, New Zealand, 13–15 February 2003.
5. Tumialan, J.G.; Morbin, A.; Micelli, F.; Nanni, A. Flexural strengthening of URM walls with FRP laminates. In Proceedings of the Third International Conference on Composites in Infrastructure (ICCI 2002), San Francisco, CA, USA, 10–12 June 2002.
6. Li, T.; Galati, N.; Tumialan, J.G.; Nanni, A. FRP strengthening of URM walls with openings-Experimental results. *ACI Struct. J.* **2005**, *4*, 569–577.
7. Silva, P.F.; Belarbi, A.; Li, T. In-plane performance assessment of URM walls retrofitted with FRP. *TMS J.* **2006**, *24*, 57–70.
8. Maria, H.S.; Alcaino, P.; Luders, C. Experimental Response of Masonry Walls Externally Reinforced with Carbon Fiber Fabrics. In Proceedings of the 8th U.S. National Conference on Earthquake Engineering, San Francisco, CA, USA, 18–22 April 2006.
9. ElGawady, M.A.; Lestuzzi, P.; Badoux, M. In-plane seismic response of URM walls upgraded with FRP. *J. Compos. Constr.* **2005**, *9*, 524–535. [[CrossRef](#)]
10. Lignola, G.P.; Prota, A.; Manfredi, G. Numerical investigation on the influence of FRP retrofit layout and geometry on the in-plane behavior of masonry walls. *J. Compos. Constr.* **2012**, *16*, 712–723. [[CrossRef](#)]
11. Pantò, B.; Cannizzaro, F.; Caddemi, S.; Calì, I.; Chàcara, C.; Lourenço, P.B. Nonlinear modelling of curved masonry structures after seismic retrofit through FRP reinforcing. *Buildings* **2017**, *7*, 79. [[CrossRef](#)]

12. Ramaglia, G.; Lignola, G.P.; Fabbrocino, F.; Prota, A. Numerical investigation of masonry strengthened with composites. *Polymers* **2018**, *10*, 334. [[CrossRef](#)]
13. Housing and Building Research Center, Egypt. *The Egyptian Code for Calculating Loads and Actions in Structural and Block Works*; ECP (201); Housing and Building Research Center: Giza, Egypt, 2012.
14. Tagel-Din, H.; Meguro, K. Applied Element Method for Dynamic Large Deformation Analysis of Structures. *Int. J. Jpn. Soc. Civ. Eng.* **2010**, *17*, 215s–224s. [[CrossRef](#)]
15. Maekawa, K.; Pimanmas, A.; Okamura, H. *Nonlinear Mechanics of Reinforced Concrete*; Spon Press: London, UK, 2003.
16. Menegotto, M.; Pinto, P. Method of analysis for cyclically loaded reinforced concrete plane frames including changes in geometry and non-elastic behavior of elements under combined normal force and bending. In *IABSE Symposium of Resistance and Ultimate Deformability of Structure acted on by Well Defined Repeated Loads*; International Association for Bridge and Structural Engineering: Zurich, Switzerland, 1973.
17. Angelillo, M.; Lourenço, P.B.; Milani, G. *Masonry Behaviour and Modelling*; Springer: Vienna, Austria, 2014; Volume 551.
18. Hartmann, D.; Breidt, M.; Nguyen, V.; Stangenberg, F.; Höhle, S.; Schweizerhof, K.; Mattern, S.; Blankenhorn, G.; Möller, B.; Liebscher, M. Structural Collapse Simulation under Consideration of Uncertainty—Fundamental Concept and Results. *Comput. Struct.* **2008**, *86*, 2064–2078. [[CrossRef](#)]
19. Giamundo, V.; Sarhosis, V.; Lignola, G.; Sheng, Y.; Manfredi, G. Evaluation of different computational modelling strategies for the analysis of low strength masonry structures. *Eng. Struct.* **2014**, *73*, 160–169. [[CrossRef](#)]
20. Pantò, B.; Cannizzaro, F.; Caliò, I.; Lourenço, P. Numerical and Experimental Validation of a 3D Macro-Model for the In-Plane and Out-Of-Plane Behavior of Unreinforced Masonry Walls. *Int. J. Arch. Heritage* **2017**, *11*, 946–964.
21. Helmy, H.; Salem, H.; Mourad, S. Computer-Aided Assessment of Progressive Collapse of Reinforced Concrete Structures according to GSA Code. *J. Perform. Constr. Facil.* **2013**, *27*, 529–539. [[CrossRef](#)]
22. Helmy, H.; Salem, H.; Mourad, S. Progressive collapse assessment of framed reinforced concrete structures according to UFC guidelines for alternative path method. *Eng. Struct.* **2014**, *42*, 127–141. [[CrossRef](#)]
23. Helmy, H.; Elfouly, A.; Salem, H. Numerical simulation of demolition of Perna Seca Hospital using the Applied Element Method. In *Proceedings of the Structures Congress, Chicago, IL, USA, 29–31 March 2012*.
24. Meguro, K.; Tagel-Din, H. AEM Used for Large Displacement Structure Analysis. *J. Nat. Disaster Sci.* **2002**, *24*, 65–82.
25. Park, H.; Suk, C.G.; Kim, S.K. Collapse Modeling of model RC Structure using Applied Element Method. *J. Korean Soc. Rock Mech.* **2009**, *19*, 43–51.
26. Salem, H. Computer-aided design of framed reinforced concrete structures subjected to flood scouring. *J. Am. Sci.* **2011**, *7*, 191–2000.
27. Salem, H.; Helmy, H. Numerical investigation of collapse of the Minnesota I-35W bridge. *Eng. Struct.* **2014**, *59*, 635–645. [[CrossRef](#)]
28. Salem, H.; Ehab, M.; Mostafa, H.; Yehia, N. Earthquake Pounding Effect on Adjacent Reinforced Concrete Buildings. *Int. J. Comput. Appl.* **2014**, *106*. [[CrossRef](#)]
29. Salem, H.; Mohssen, S.; Kasa, K.; Hosoda, A. Collapse Analysis of Utatsu Ohashi Bridge Damaged by Tohoku Tsunami using Applied Element Method. *J. Adv. Concr. Technol.* **2014**, *12*, 388–402. [[CrossRef](#)]
30. Tagel-Din, H. Collision of Structures during Earthquakes. In *Proceedings of the 12th European Conference on Earthquake Engineering, London, UK, 9–13 September 2002*.
31. Asprone, D.; Nanni, A.; Tagel-Din, H. Applied Element Method Analysis of Porous GFRP Barrier Subjected to Blast. *Adv. Struct. Eng.* **2010**, *13*, 153–169. [[CrossRef](#)]
32. Almusallam, T.H.; Elsanadedy, H.M.; Abbas, H.; Ngo, T.; Mendis, P. Numerical analysis for progressive collapse potential of a typical-framed concrete building. *Int. J. Civ. Environ. Eng.* **2010**, *10*, 36–42.
33. Kang, H.; Kim, J. Progressive Collapse of Steel Moment Frames Subjected to Vehicle Impact. *J. Perform. Constr. Facil.* **2015**, *29*, 6. [[CrossRef](#)]
34. Griffin, J.W. Experimental and Analytical Investigation of Progressive Collapse through Demolition Scenarios and Computer Modeling. Master's Thesis, Civil Engineering, Raleigh, NC, USA, 2008.

35. Extreme Loading of Structures (ELS). Available online: <http://www.extremeloading.com> (accessed on 10 January 2018).
36. Gasprini, D.A.; Vanmarcke, E.H. *SIMQKE User's Manual and Documentation*; Massachusetts Institute of Technology: Cambridge, MA, USA, 1976.



© 2018 by the authors. Licensee MDPI, Basel, Switzerland. This article is an open access article distributed under the terms and conditions of the Creative Commons Attribution (CC BY) license (<http://creativecommons.org/licenses/by/4.0/>).